Available online at www.sciencedirect.com
SCIENCE DIRECT®
Journal of Nuclear Materials 354 (2006) 143–162
journal of nuclear materials
www.elsevier.com/locate/jnucmat

Crystallization of neodymium-rich phases in silicate glasses developed for nuclear waste immobilization

D. Caurant [a,*], O. Majerus [a], P. Loiseau [a], I. Bardez [a], N. Baffier [a], J.L. Dussossoy [b]

[a] Laboratoire de Chimie Appliquée de l'Etat Solide (UMR CNRS 7574), ENSCP, 11 rue Pierre et Marie Curie, 75231 Paris, France
[b] CEA Valrho, DTCD/SCDV/LEBV, 30207 Bagnols-sur-Cèze, France

Received 31 January 2006; accepted 27 March 2006

Abstract

Glass-ceramics containing neodymium-rich crystalline phases can be obtained by crystallization of silicate glasses (nucleation + crystal growth heat treatments) or by controlled cooling of melts. Such materials could be envisaged as durable matrices for conditioning minor actinides- and Pu-rich nuclear wastes if the partitioning ratio of the wastes between crystalline phase and residual glass is high (principle of double containment barrier). In radioactive waste forms, Nd would be partially substituted by actinides and neutron absorbers (Gd). In this work, two silicate glass compositions leading to efficient nucleation and crystallization of either zirconolite ($Ca_{1-x}Nd_xZrTi_{2-x}Al_xO_7$, $x < 1$) or apatite ($Ca_2Nd_8Si_6O_{26}$) in their bulk were studied as potential waste forms. The effect of the method used to prepare glass-ceramics (controlled cooling from the melt or nucleation + crystal growth from the glass) on both the microstructure and the structure of the neodymium-rich crystalline phase was studied. The highest number of zirconolite or apatite crystals in the bulk was obtained using the nucleation + crystal growth method. However, the percentage of neodymium incorporated in zirconolite crystals remained too small to make realistic the use of such materials for the conditioning of actinides in comparison with more durable bulk ceramics.

PACS: 81.05.Kf; 61.43.Fs; 81.05.Pj; 64.60.Qb

1. Introduction

Reprocessing of nuclear spent fuel by the Purex process, performed in order to recover U and Pu, generates high level nuclear waste solutions (HLW) containing fission products and long-lived minor actinides MA (Np, Am, Cm). MA represent only a small fraction (2–3 wt%) of the waste formed in the spent fuel in comparison with fission products (97–98 wt%) [1,2]. Currently, MA are not separated from the other radioactive or non-radioactive elements in HLW, they are immobilized with the fission products in glassy (mainly borosilicate) matrices after melting and casting. In these glasses MA concentration is very low, for instance MA reach less than 0.4 wt% in the French nuclear glass R7T7 [3] but

* Corresponding author. Tel.: +33 1 53737922; fax: +33 1 46347489.
E-mail address: daniel-caurant@enscp.fr (D. Caurant).

0022-3115/$ - see front matter © 2006 Elsevier B.V. All rights reserved.
doi:10.1016/j.jnucmat.2006.03.014

one knows how to increase this amount if required using for instance rare earth-rich glasses.

MA are long-lived α-emitting radionuclides that will be mainly responsible for the long-term potential radiotoxicity of the glass waste forms after 2–3 hundred years in a repository [1]. To minimize the potential long-term impact of HLW, investigations are currently in progress in several countries such as in France about the enhanced separation of MA from HLW followed by their transmutation or their immobilization in specific very highly durable host matrices such as ceramics [4–6]. Indeed, it is known that several ceramics such as zirconates, titanates and phosphates may incorporate high amounts of MA in their structure and exhibit very good chemical resistance against water [5–8]. Highly durable matrices are also under development for Pu-rich military wastes immobilization [7,9]. Nevertheless, it must be underlined that glassy matrices remain the best waste forms for the simultaneous immobilization of all the elements (more than 40) existing in HLW and that the R7T7 glass in disposal will exhibit a long-term durability higher than 10^5 years.

Among the different matrices investigated for the specific immobilization of MA and Pu, the single phase ceramics zirconolite and fluorophosphosilicate apatite exhibit very high chemical durability and have been widely studied [6,9,10]. The existence in nature of very old zirconolite and apatite minerals that have successfully retained U and/or Th even thought they have been rendered metamict by alpha decay, is generally considered as a good indication of their excellent long-term behavior (i.e. the effects of radiation-induced damage on their chemical stability were minimal) and explains why these phases are envisaged to securely immobilize Pu and MA for several thousands of years. The possibility to incorporate high amounts of actinides and lanthanides (considered as good surrogates at least for the heaviest MA as indicated below) in these ceramics was demonstrated. For instance, following the compensation charge scheme $[Ca_{1-x}Nd_x]Zr[Ti_{2-x}Al_x]O_7$ (with the Al^{3+} ions located in Ti sites acting as charge compensators for the Nd^{3+} ions incorporated in Ca site), it was shown that zirconolite (nominally $CaZrTi_2O_7$) can incorporate neodymium amounts as high as $x = 0.6$ without structural changes [10]. Following the same scheme, it was shown that zirconolite can accept nearly 0.4 Pu^{3+} ions (in Ca site) by formula unit [11]. It was also demonstrated that ceramics such as fluorophosphosilicate apatites $(Ca_{10-y}Nd_y(SiO_4)_y(PO_4)_{6-y}F_2,\ y > 0)$ and silicate apatites $Ca_2Ln_8(SiO_4)_6O_2$ (with Ln = Nd or Gd) can be prepared with MA or Pu partly replacing Ln in the structure [8,12,13].

It is important to point out that trivalent lanthanide ions (such as Nd^{3+} ions in this study) are good surrogates only for the heaviest transuranic elements occurring in HLW such as Am and Cm. Indeed, these two actinide elements occur as trivalent ions in glasses [14,15] and have cation radii r similar to the one of Nd^{3+} ion (for instance in sixfold coordination: $r(Am^{3+}) = 0.0975$ nm and $r(Nd^{3+}) = 0.0983$ nm [16]). In comparison, the other actinide elements of HLW (U, Np, Pu) generally occur under oxidation state higher than +III in glasses. For instance, plutonium mainly occurs as Pu^{4+} ions in nuclear glasses prepared under neutral or oxidizing conditions [17]. Thus, trivalent lanthanides are not good Pu surrogates except if the Pu containing glasses are prepared under strongly reducing conditions (using for instance strong reducing agent such as Si_3N_4 in the melt [18] almost all Pu^{4+} ions can be reduced to Pu^{3+} ions). The behavior differences between the heaviest and the lightest actinides of HLW are due to the increase of the nuclear charge for the heaviest actinide elements which affect the energy and the spatial extension of 5f orbitals.

Radioactive single-phase ceramic waste forms remain difficult to prepare (grinding + sintering) than radioactive glasses (melting + casting) in nuclear facilities. To benefit at the same time from the ease of glass preparation and from the very good long-term behavior of ceramics, the preparation of glass-ceramic waste forms consisting of small zirconolite or apatite crystals (which would preferentially incorporate MA or Pu) homogeneously dispersed in a durable glassy matrix – acting as a second barrier of containment – appears as an interesting alternative (double containment principle). However, for such an application, wastes need to be incorporated with a strong partitioning ratio in the crystalline phase. Moreover, due to the existence of a residual glassy phase embedding the crystals, glass-ceramics could accommodate more easily waste composition fluctuations and impurities than ceramics. Indeed, because of the crystalline structure of ceramics, impurities and waste composition fluctuations could generate low durability parasitic phases containing radioactive elements in ceramic waste forms.

The aim of this work was to study and to control the crystallization of neodymium-rich phases (zirconolite and apatite) in two parent glasses (A and B) belonging to different systems and containing high Nd_2O_3 concentrations in order to prepare glass-ceramics. In our previous works [19–26], these two glasses were shown to lead, respectively, to the crystallization of zirconolite and apatite in their bulk. To complete the characterization of glass-ceramic B, three other glasses (C, D, E) whose compositions were derived to the one of glass B were prepared and crystallized.

For parent glass A belonging to the SiO_2–Al_2O_3–CaO–TiO_2–ZrO_2–Nd_2O_3 system, the possibility to prepare zirconolite-based glass-ceramics containing zirconolite crystals in their bulk (internal nucleation) was demonstrated [19–24]. In all these studies, the glass-ceramics were prepared by controlled crystallization: nucleation near glass transformation temperature $T_g \sim 760$ °C + crystal growth at higher temperature 1000–1200 °C. In the zirconolite crystals of these glass-ceramics, it was shown that Nd^{3+} ions were preferentially incorporated into the Ca site of the structure. However, the simultaneous formation of a thin crystallized layer containing mainly titanite (nominally $CaTiSiO_5$ also known as sphene) and anorthite (nominally $CaAlSi_2O_8$) was observed on the surface of the glass-ceramic samples. Among these two silicate crystalline phases nucleating on the glass surface, only titanite was shown to be able to incorporate lanthanides [23]. For parent glass B, belonging to the SiO_2–B_2O_3–Al_2O_3–Na_2O–CaO–ZrO_2–Nd_2O_3 system, a strong crystallization tendency of Nd-silicate apatite with composition near $Ca_2Nd_8(SiO_4)_6O_2$ was observed [25,26]. It must be pointed out that the zirconolite phase is known to exhibit both a higher chemical durability and a lower radiation-induced swelling than the Nd-silicate apatite phase [27], thus zirconolite-based glass-ceramics would probably exhibit better long-term behavior than Nd-silicate apatite based ones.

In the first part of the work reported here, we studied how the crystallization of the silicate phases (anorthite, titanite) from glass A surface could compete with zirconolite crystallization in the bulk according both to the method used to crystallize the samples (controlled cooling from the melt or thermal treatment of the parent glass) and to the temperature (T_c) and the duration (τ) of the crystal growth thermal treatment. In the second part of this work, the study of the crystallization of apatite in glass B either during slow cooling of the melt or after heating (nucleation + crystal growth) of the glass is presented.

2. Experimental methods

The compositions of glasses A and B studied in this work are the following (mol.%): SiO_2 (48.23), Al_2O_3 (8.37), CaO (25.01), ZrO_2 (4.90), TiO_2 (11.14), Na_2O (1.08), Nd_2O_3 (1.27) (glass A); SiO_2 (61.81), B_2O_3 (8.94), Al_2O_3 (5.95), Na_2O (12.40), CaO (5.44), ZrO_2 (1.89), Nd_2O_3 (3.56) (glass B). The compositions listed here correspond to the target compositions. The aimed Nd_2O_3 concentrations are 6.0 and 16.0 wt%, respectively, for glasses A and B. All glass samples were analyzed by the ICP-AES method at the CNRS Service Central d'Analyses (Vernaison, France).

The high TiO_2 and ZrO_2 concentrations in glass A were introduced in order to promote zirconolite crystallization [23,28]. The lack of boron, the very low amount of sodium and the significant amounts of zirconium, titanium, calcium and aluminum in glass composition suggest a high chemical durability both for the parent glass and for the corresponding glass-ceramics obtained after partial crystallization. Na_2O and B_2O_3 were introduced in glass B in order to reduce its melting temperature (1300 °C) for technological reasons [25,26].

All the samples (≈50 g) prepared for the study of crystallization of glass A were prepared using reagent-grade SiO_2, $CaCO_3$, Na_2CO_3, Al_2O_3, TiO_2, ZrO_2 and Nd_2O_3 powders. The batch was melted at 1550 °C for 10 h in a Pt crucible, poured in water and ground (particle size < 800 μm) before remelting (1550 °C for 4 h) in order to obtain a highly homogeneous glass. Three different crystallization methods (Fig. 1) were investigated to prepare zirconolite-based glass-ceramics. For the three methods, the samples were transferred very rapidly in furnaces preheated at the corresponding temperatures. As shown below, these methods led to samples containing different amounts of zirconolite and silicate (titanite and anorthite) crystals:

– The first method (method 1, Fig. 1(a)) consists of controlled cooling of the melt from 1550 °C to room temperature without any nucleation stage before the crystal growth stage at T_c. This crystal growth stage was performed directly by rapid cooling of the melt from 1550 °C to T_c = 1200 °C or 1050 °C. The samples were kept at

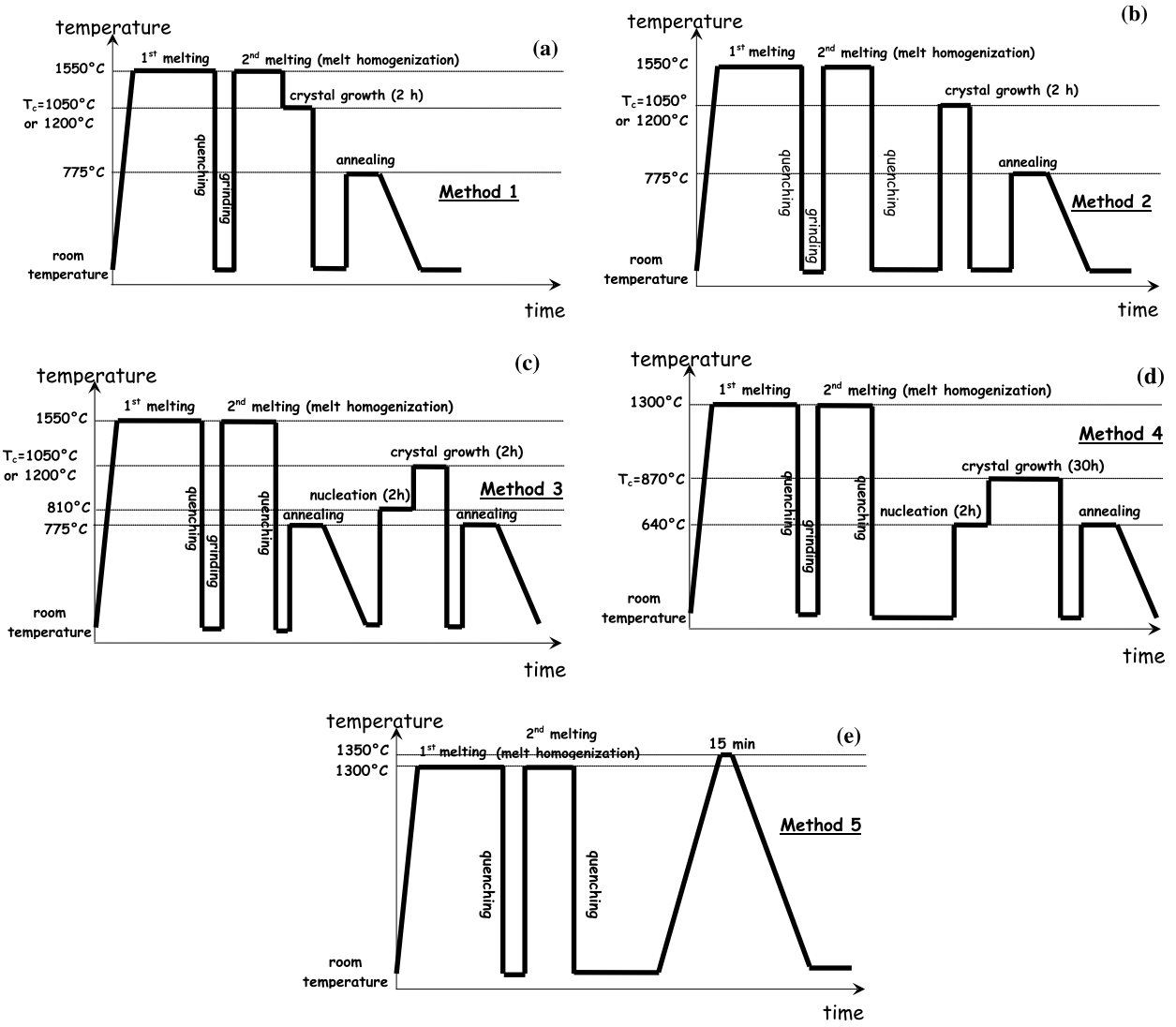

Fig. 1. Schemes $T = f(\text{time})$ showing the different stages of glass-ceramics preparation from glass A and B compositions using methods: glass A (1 (a), 2 (b), 3 (c)); glass B (4 (d) and 5 (e)). The positions (time, T) indicated on the two axes are only qualitative.

T_c for 2 h and then quenched to room temperature in the platinum crucible without casting. In previous studies [19–23], the two T_c temperatures used in this work (1050 °C and 1200 °C) were shown to lead to the crystallization of only zirconolite in the bulk of glass samples previously submitted to a nucleation stage (see method 3 below).

– The second method (method 2, Fig. 1(b)) consists of heating directly (in small Pt crucibles) at $T_c = 1050$ °C or 1200 °C for 2 h, the glass samples previously prepared by quenching the melt from 1550 °C to room temperature (without subsequent annealing or nucleation stages). The samples were then quenched to room temperature.

– The third method (method 3, Fig. 1(c)) is the one used in previous studies [19–24]. The glass-ceramic samples were prepared using annealed glass (775 °C for 2 h) submitted to nucleation and crystal growth thermal treatments (in small Pt crucibles) at, respectively, $T_n = 810$ °C for 2 h (the maximum of the nucleation rate curve $I = f(T)$ was reached for $T = 790$ °C [19]) and $T_c =$ 1050 °C or 1200 °C for 2 h. The samples were then quenched to room temperature. As nucleation probably also occurred during annealing, method 3 could be presented as a cycle with two nucleation treatments (2 h at 775 °C then 2 h at 810 °C) instead of annealing + nucleation.

For methods 2 and 3, the melt was initially cast in steel molds to form small glass cylinders (14 mm diameter and 10 mm high). In order to study the stability at high temperature of the glass-ceramics prepared following method 3, and more specially to follow the competition between internal and surface crystallization, the effect of the crystal growth thermal treatment duration τ at 1050 °C (from 2 h to 300 h) and 1200 °C (from 2 h to 20 h) was studied. All the samples obtained after the crystallization thermal treatments of glass A were annealed at 775 °C (15 °C higher than T_g) for 2 h before slow cooling in order to relieve the internal stresses before cutting with a diamond saw.

Glass B (≈50 g) was melted at 1300 °C for 3 h in a platinum crucible using reagent-grade SiO_2, $CaCO_3$, Na_2CO_3, H_3BO_3, Al_2O_3, ZrO_2 and Nd_2O_3 powders. As for glass A, the melt was then poured in water and ground before remelting (1300 °C for 2 h) in order to obtain a more homogeneous glass. The melt was then cast in steel molds to form small glass cylinders similar to the ones of glass A. Due to the occurrence of significant amounts of Na_2O (12.40 mol.%) and B_2O_3 (8.94 mol.%) in glass B, this glass could be prepared at lower temperature than glass A. Indeed, boron and sodium oxides are known to decrease melt viscosity and liquidus temperature of glass compositions. Moreover, in order to reduce the risks of boron and sodium evaporation during melting, the total duration of melting stage (5 h) was shorter than for glass A (14 h). For glass B, only two crystallization methods were compared. The first one (method 4, Fig. 1(d)) has similarities with the method 3 used for glass A: nucleation and crystal growth thermal treatments on glass B cylinders in small Pt crucibles at, respectively, $T_n = 640$ °C for 2 h and $T_c = 870$ °C for 30 h. The samples were then quenched to room temperature. As only one kind of crystalline phase was observed for this composition (i.e., apatite in the bulk and near glass surface), the stability of the glass-ceramics for long thermal treatments was not studied. Contrarily to glass A, the maximum of the nucleation rate curve for glass B was unknown but we choose to perform the nucleation heat treatment at $T_g + 20$ °C (640 °C). Indeed, it is known that in glasses, the maximum of the internal volume nucleation rate often occurred near T_g [29]. The value of T_c was chosen according to the position of the exothermic effect on differential thermal analysis curves. The second crystallization method (method 5, Fig. 1(e)) performed on glass B, corresponds to slow cooling (6 °C/min) from the melt at 1350 °C to room temperature. For this method, samples of glass B (placed in Pt crucibles) were introduced in a furnace at room temperature and then heated (6 °C/min) to 1350 °C during 15 min before slow cooling. In order to destroy the crystals that could nucleate and grow during the heating of glass B at 6 °C/min, it was decided to increase the melt temperature by 50 °C before slow cooling (Fig. 1(e)). To complete the study of glass B, the following three glasses C, D and E with compositions derived from the one of glass B were prepared using the same preparation method: (mol.%): SiO_2 (61.81), B_2O_3 (8.94), Al_2O_3 (3.05), Na_2O (14.41), CaO (6.33), ZrO_2 (1.89), Nd_2O_3 (3.59) (glass C); SiO_2 (53.7), B_2O_3 (9.3), Al_2O_3 (9.6), Na_2O (15.1), CaO (6.6), ZrO_2 (2.0), Nd_2O_3 (3.7) (glass D); SiO_2 (53.7), B_2O_3 (9.3), Al_2O_3 (9.6), Na_2O (21.7), CaO (0), ZrO_2 (2.0), Nd_2O_3 (3.7) (glass E).

All the samples were characterized by X-ray diffraction (XRD) with a Siemens D5000 apparatus operating at Co K_α wavelength ($\lambda = 0.1778897$ nm). The crystallized phases formed in the bulk or near the surface of the samples (glass A) were separated by cutting with a diamond saw and studied separately by XRD. The glass-ceramics were also studied by scanning electron microscopy (SEM) on polished and carbon coated samples with a Hitachi S2500 microscope. For glass A, all samples obtained after crystallization (methods 1–3) were analyzed quantitatively by energy dispersive X-ray analysis (EDX) with a PGT analyzer (accelerating voltage 15 kV, beam current ≈1.8 nA) coupled with the SEM. Such EDX analysis were only performed for the glass-ceramic samples prepared at $T_c = 1200$ °C for which crystals were large enough to be probed by the microscope electron beam. For glass B, the apatite crystals were too small to be analyzed quantitatively by EDX. However, for glass C, it was possible to determine by EPMA (electron probe microanalysis) the composition of the apatite crystals formed after slow cooling (1 °C/min) due to their size relatively large. In order to determine both T_g (determined as the onset of the corresponding endothermic effect) and the temperature range of exothermic effects associated with crystallization, differential thermal analysis (DTA) experiments were performed on glasses A and B with the help of a STA409 Netzsch thermal analysis apparatus (heating rate: 10 °C/min).

3. Results and discussion

Glass A and B samples obtained after quenching of the melt at room temperature were optically clear and X-ray powder diffraction showed that they were amorphous. They exhibit the characteristic blue-purple color associated with Nd^{3+} ion f–f transitions. Chemical analysis of glass A indicated only slight deviations from nominal composition ((mol.%): SiO_2 (47.18), Al_2O_3 (8.72), CaO (24.96), ZrO_2 (5.04), TiO_2 (11.54), Na_2O (1,26), Nd_2O_3 (1,30)). However, for glass B, the results showed depletions with respect to the nominal composition concerning boron (7–9 mol.%) and sodium (5–10 mol.%) concentrations due to the volatility of these elements during melting. The DTA curves associated with the two glasses are shown in Fig. 2. The glass transformation temperature (T_g) of glasses A and B were, respectively, 760 and 620 °C (± 5 °C). In spite of high concentrations of network forming oxides (SiO_2, Al_2O_3, B_2O_3) in glass B in comparison with glass A, we observed that T_g (glass A) > T_g (glass B). The high amount of low field strength Na^+ modifier cations (in comparison with the high amount of high field strength Ca^{2+} modifier cations in glass A) and the occurrence of a high proportion of triangular BO_3 units (>60% of all the boron units [25]) in glass B could explain the T_g difference between the two glasses [30].

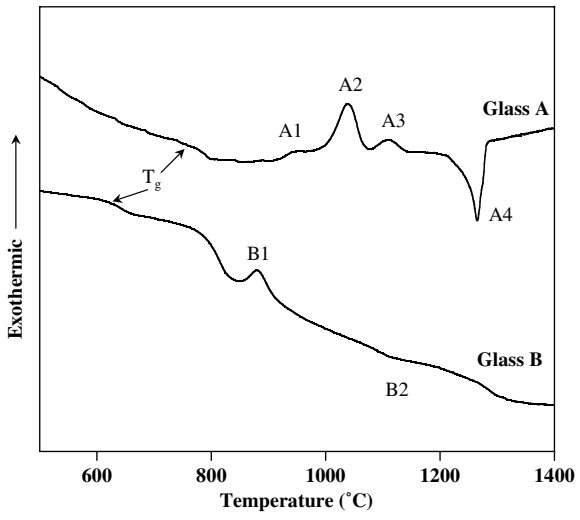

Fig. 2. DTA curves of A (particle size 125–200 μm) and B (particle size 80–125 μm) glasses. The position of T_g (onset of the endothermic effect) is shown for the two glasses. For glass A, the A1, A2 and A3 exothermic peaks were associated, respectively, to highly disordered zirconolite (defect fluorite structure phase), titanite and anorthite surface crystallization [32]. For glass B, the exothermic effect B1 was associated with apatite crystallization. Endothermic effects A4 and B2 are due to the melting of the crystalline phases.

3.1. Study of the crystallization of zirconolite from glass A

Comparison by XRD, SEM and EDX of the different samples obtained from glass A using the three crystallization methods showed strong differences concerning both the nature of the crystalline phases and the microstructure of the glass-ceramics. The existence of differences between crystallization phenomena occurring during melt cooling and glass heat treatment was also reported by Hayward [31] in his study on titanite-based glass-ceramics. The exothermic effects A1, A2 and A3 observed on the DTA curve of glass A (Fig. 2) were shown – by XRD – to be due to the crystallization from the surface of the glass particles of, respectively, highly disordered zirconolite (defect-fluorite structure), titanite and anorthite [32]. The endothermic effect A4 was associated with the melting of the crystalline phases at higher temperature.

3.1.1. Crystallization during controlled cooling of the melt (method 1)

Crystallization following method 1 gives essentially zirconolite (Z) crystals which have grown after nucleation on the sample surface (Fig. 3(a) and (b); heterogeneous nucleation) and form a crystallized layer whose thickness reached 100 and 1000 μm at, respectively, 1050 and 1200 °C. Due to heavy elements (Zr, Nd) enrichment in zirconolite in comparison with residual glass, the crystals appeared as a white phase with a strong contrast on back-scattered electrons SEM images (Fig. 3). The composition of the zirconolite crystals (formed at T_c = 1200 °C, method 1) determined by EDX is given in Table 1. The nature of the crystals was determined using both XRD and EDX. The XRD patterns of the crystalline layer formed near the surface (T_c = 1200 °C) is shown in Fig. 4(a) and the corresponding lattice parameters are given in Table 2. The cell parameters of the $Ca_{0.8}Nd_{0.2}ZrTi_{1.8}Al_{0.2}O_7$ ceramic prepared by solid state reaction [10] from reagent grade powders ($CaCO_3$, ZrO_2, TiO_2, Al_2O_3, Nd_2O_3) are also given in this table for comparison. The composition of this ceramic was chosen in accordance with the composition (EDX results) of the zirconolite crystals formed at T_c = 1200 °C in glass A (Table 1). It appeared that

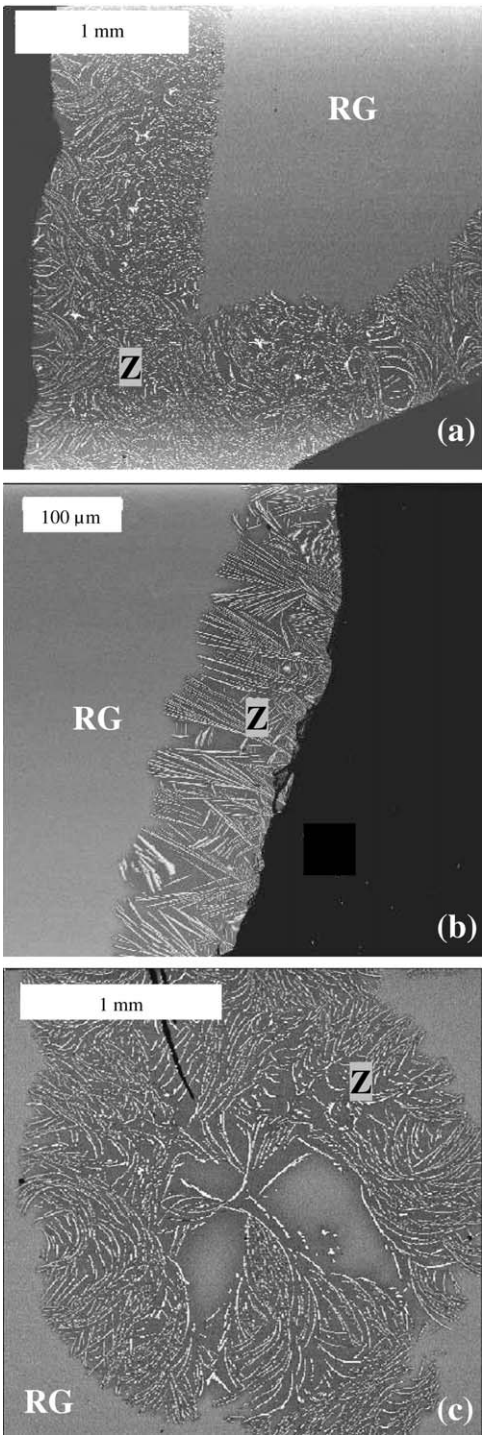

Fig. 3. Back-scattered SEM images of the samples obtained after heat treatment of glass A following method 1 at $T_c = 1200$ °C (surface (a), bulk (c)) and $T_c = 1050$ °C (surface (b)). Z, zirconolite; RG, residual glass.

the cell parameters of the zirconolite ceramic and of the crystals formed in glass A using method 1 were very similar. Whereas no crystals were detected by SEM in the bulk of the samples prepared at $T_c = 1050$ °C, only zirconolite crystals (with spherulitic shape and approximately 2 mm diameter) were shown to form in the bulk at 1200 °C (Fig. 3(c)). The corresponding weak intensity XRD pattern shown in Fig. 4(b) confirmed that the crystals formed in the bulk are the same as the ones nucleating on surface. However, the number of zirconolite crystals in the bulk was very small. They probably nucleated on sporadic sites preexisting in the melt (impurities, bubbles,...) rather than homogeneously. Consequently, the amount of residual glass in the bulk remained very high after 2 h of crystal growth (Fig. 3). The fact that the mol.% amounts of Nd^{3+} and Al^{3+} ions in the zirconolite crystals are nearly the same shows that neodymium ions are preferentially incorporated in the calcium site of the structure whereas aluminum ions (incorporated in titanium sites) totally compensate the positive charge excess induced by the incorporation of neodymium. The slight amount of silicon detected by EDX probably originated from a small contribution to the EDX spectra of the residual glass around the crystals. Because of the small quantity of crystals formed in their bulk, the samples obtained following method 1 cannot be considered as true glass-ceramics and this method cannot be applied without significant modifications to the immobilization of actinides. As shown below (method 3), an intermediate zirconolite nucleation stage at lower temperature (near 800 °C) before crystal growth is necessary in order to increase the amount of zirconolite in the bulk. The fact that zirconolite nucleated essentially heterogeneously for $T \geqslant 1050$ °C is in accordance with the zirconolite homogeneous nucleation rate

Table 1
Composition determined by EDX of the zirconolite crystals formed in bulk of the samples obtained after partial crystallization of glass A, following methods 1, 2 and 3 ($T_c = 1200$ °C)

Crystallization method	Crystals composition
Method 1	$Ca_{0.84}(Nd_{0.18})Zr_{0.97}Ti_{1.72}(Al_{0.17})Si_{0.12}O_{6.99}$
Method 2	$Ca_{0.82}(Nd_{0.19})Zr_{1.06}Ti_{1.70}(Al_{0.16})Si_{0.06}O_{6.99}$
Method 3	$Ca_{0.82}(Nd_{0.19})Zr_{1.08}Ti_{1.67}(Al_{0.18})Si_{0.06}O_{7}$

The slight amount of silicon detected in the zirconolite crystals probably originates from a weak contribution of the residual glass to EDX spectra. Due to the too small size of the zirconolite crystals formed in the samples prepared at $T_c = 1050$ °C, it was not possible to analyze these crystals without a strong contribution of the residual glass (these analysis are thus not given in this table).

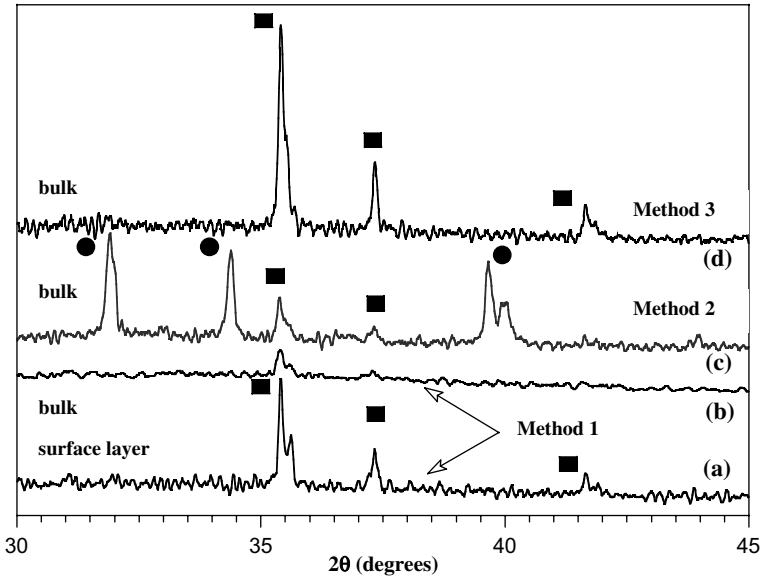

Fig. 4. XRD patterns of samples obtained after heat treatments of glass A ($T_c = 1200$ °C, 2 h) using: method 1 (crystallized surface layer (a), bulk (b)); method 2 (bulk (c)) and method 3 (bulk (d)). ■, Zirconolite; ●, Titanite. (λCo K_α: 0.178897 nm).

Table 2
Unit cell parameters (a, b, c, β) of the monoclinic zirconolite crystals formed in the samples obtained after partial crystallization of glass A, following methods 1 and 3 ($T_c = 1200$ °C)

	a (nm)	b (nm)	c (nm)	β (°)
Zirconolite (method 1)	1.2482(2)	0.7276(1)	1.1376(1)	100.60(1)
Zirconolite (method 3)	1.2512(2)	0.7267(1)	1.1374(2)	100.63(2)
Zirconolite (ceramic) $Ca_{0.8}Nd_{0.2}$ $ZrTi_{1.8}Al_{0.2}O_7$	1.24685(7)	0.72697(4)	1.13589(6)	100.654(5)

The parameters were deduced from the indexation of XRD patterns in the $C2/c$ space group (zirconolite-2M polytype). For comparison the cell parameters of the $Ca_{0.8}Nd_{0.2}ZrTi_{1.8}Al_{0.2}O_7$ ceramic are given. This ceramic was prepared by solid state reaction at 1400 °C for 100 h (first sintering) and then at 1460 °C for 100 h after grinding and peletizing (second sintering) [10]. Numbers in parentheses are standard deviations and applied to the last quoted place.

$I_Z^{hom}(T)$ and crystal growth rate $u_Z(T)$ curves reported in our previous studies [22] which showed that zirconolite bulk nucleation and crystal growth occurred in two well separated temperature ranges and the maximum of $I_Z^{hom}(T)$ occurred near 790 °C $\ll T_c$. Thus, at high temperature ($T_c \geqslant 1050$ °C) $I_Z^{hom}(T) \approx 0$ and $I_Z^{het}(T) \gg I_Z^{hom}(T)$. This is in agreement with the general tendency of the nucleation thermodynamic barrier to decrease near interfaces [29,33]. Moreover, the study of the sample prepared following method 1 showed that titanite (S) and anorthite (A) heterogeneous nucleation rates (respectively, $I_S^{het}(T)$ and $I_A^{het}(T)$) were negligible for $T_c = 1050$ °C and 1200 °C (only scarce titanite crystals were detected near sample surface for $T_c = 1050$ °C). All these results showed that: $I_Z^{het}(T) > I_S^{het}(T)$, $I_A^{het}(T) \approx 0$ for $T \geqslant 1050$ °C.

3.1.2. Crystallization by the mean of a single crystal growth stage (method 2)

Using method 2 for the crystallization of glass A, strong nucleation of titanite and anorthite crystals on glass surface followed by their growth towards the bulk was observed at the expense of zirconolite (no zirconolite crystals were observed near sample surface) (Fig. 5(a) and (c)). The composition of the zirconolite crystals formed in the bulk (Fig. 5(b)) using method 2 ($T_c = 1200$ °C) was very similar to the one determined above for method 1 (Table 1). Due to the lack of heavy elements (such as Zr, Nd) in anorthite crystals, they appeared as a black phase on the back-scattered electrons SEM images in comparison with both titanite crystals (white) and residual glass (grey). Indeed, contrary to anorthite, titanite was shown to incorporate Nd in its structure

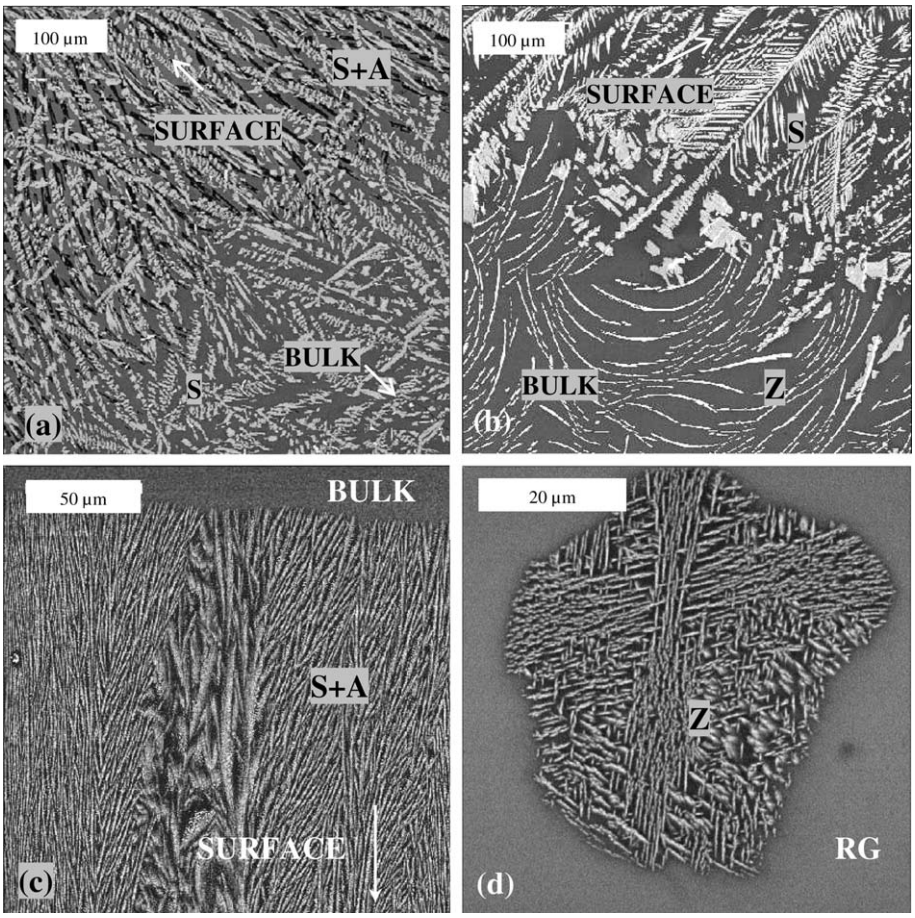

Fig. 5. Back-scattered SEM images of the samples obtained after heat treatment of glass A following method 2 at $T_c = 1200$ °C (near surface (a), near bulk (b)) and $T_c = 1050$ °C (near surface (c), bulk (d)). Z, zirconolite; RG, residual glass; S, titanite (appearing as elongated crystals with dendritic shape); A, anorthite (appearing as dark and elongated crystals in (a)).

[20]. Hayward [31] also indicated that in its precursor glasses developed for the preparation of titanite-based glass-ceramics, titanite crystals preferentially nucleated heterogeneously on glass surface or from boundaries between separated glass phases. Nevertheless, for glass A no glass-in-glass phase separation was observed by electron microscopy even after prolonged nucleation heat treatment [22]. In comparison with method 1, only a small increase of the quantity of zirconolite crystals nucleated in the bulk was observed for method 2, but this phase still remained the only one to nucleate in the bulk (Fig. 5(b) and (d)). The origin of these differences of nucleation behavior in the bulk between zirconolite in one hand and titanite and anorthite in the other hand is not well understood. It could be due to the fact that – contrary to anorthite and titanite – zirconolite contains high proportions of both TiO_2 and ZrO_2. Indeed, these two oxides are well known for their nucleating effect in glasses due to the high field strength of Ti^{4+} and Zr^{4+} ions [33] which is at the origin of their tendency to separate from glasses during heat treatments. The sample obtained after thermal treatment at $T_c = 1200$ °C (method 2) contained a high quantity of titanite and anorthite crystals that have grown from the surface toward the bulk (Fig. 5(a) and (b)). For $T_c = 1200$ °C the thickness of the titanite + anorthite crystallized layer reached 2–3 mm in comparison with only 1 mm for $T_c = 1050$ °C. Comparison of the size of the different crystals growing either in the bulk (Z) or from the surface (S, A) indicated that the corresponding growth rates $u(T)$ could be ordered as follows: $u_S(T) > u_A(T) \gg u_Z(T)$. Indeed, Fig. 5(a) and (b) clearly showed that at $T_c = 1200$ °C, the growth of titanite from the surface toward the bulk was higher than for anorthite. The XRD pattern shown in Fig. 4(c) was obtained after cutting and elimination of a thin surface layer.

In this pattern, the intensity of the lines associated with titanite is high which is in agreement with the strong growth of titanite crystals toward the bulk. The fact that the crystal growth rate of zirconolite was considerably smaller than the one of the two other silicate phases can be explained from kinetics considerations as follows. As silicon does not enter in zirconolite according to EDX results, SiO_2 is totally rejected in the residual glass near the crystals during their growth at T_c. This is not the case for anorthite and titanite crystals because silica is one of the main oxides entering in their composition. Consequently, it can be understood that the diffusional and reconstructive phenomena occurring during crystals growth are more slowed down for zirconolite than for the two other phases. In comparison with method 1, titanite and anorthite heterogeneous nucleation on sample surface strongly increased using method 2. This showed that the heterogeneous nucleation of these two phases occurred very quickly during melt quenching and/or during glass heating: it is likely to happen in a temperature range slightly higher than T_g, where nucleation rate is known to be the highest [29]. The differences observed between zirconolite and the two silicate phases concerning their nucleation rate on sample surface thus showed that: $I_S^{het_{max}} \gg I_Z^{het_{max}}$ and $I_A^{het_{max}} \gg I_Z^{het_{max}}$ where the subscript max refers to the maximum nucleation rate. This implies that even a short stay of the undercooled melt in the temperature range where $I_T^{het}(T)$ and $I_A^{het}(T)$ are very high ($T_g < T < 1050$ °C) would then induce a strong effect concerning the nature of the crystalline phases growing from the surface at T_c. Thus, in order to avoid the crystallization of a high quantity of silicate phases from the surface toward the bulk of glass A, the undercooled melt must to be kept at a temperature at least higher than 1050 °C during the process, except if a prolonged nucleation heat treatment is performed near $I_Z^{hom_{max}}$ as shown below for method 3. It is interesting to indicate here that a study of the crystallization of zirconolite in iron-enriched basalt glasses (with 5 wt% of both TiO_2 and ZrO_2) by isothermal treatments without nucleation stage (as in method 2 in our work) between 1000 and 1200 °C for 24 h was reported in the literature [34]. This work was performed in order to develop waste forms to immobilize transuranic elements (simulated by lanthanides mixture) occurring in low-level waste. As in our case, actinides were aimed to be incorporated in the zirconolite phase. It was shown that zirconolite was formed in the bulk but additional crystalline phases (spinel, pyroxene, and plagioclase for instance) were also observed in the residual glass.

3.1.3. Crystallization by the mean of a nucleation stage followed by a growing stage (method 3)

Methods 1 and 2 lead only to a very small quantity of zirconolite crystals in the bulk of the glass due to the lack of a specific nucleation stage for this phase. This amount could be strongly increased using method 3 for which nucleation stages at 775 °C (annealing) and 810 °C were performed (Fig. 6(a) and (c)). The results concerning this method were already described in details in [23]. Following this method, only zirconolite nucleated in the bulk showing that $I_Z^{hom}(T) \gg I_S^{hom}(T), I_A^{hom}(T)$. In this case, the growth of the titanite + anorthite surface layer towards the bulk of the samples was considerably slowed down due to the high density of small zirconolite crystals (size < 10–20 μm) formed in the bulk (Fig. 6(c) and (d)): the surface crystallized layer reached a thickness of 200 and 850 μm, respectively, for $T_c = 1050$ °C and 1200 °C. Comparison of Figs. 5(d) and 6(c) showed a significant decrease of the zirconolite (dendritic shape) crystals size in the bulk between methods 2 and 3. This difference could be explained by the high number of nuclei formed in the bulk of glass A during nucleation using method 3. This induced rapidly an impingement of the crystals during the growth heat treatment at T_c.

The composition of the zirconolite crystals formed in the bulk for $T_c = 1200$ °C is given in Table 1. It appeared that this composition remained almost constant for the three methods: nearly 20% of the zirconolite Ca sites were occupied by Nd^{3+} ions with charge compensation ensured by Al^{3+} ions into the Ti sites. The lattice parameters of the zirconolite crystals formed in the bulk ($T_c = 1200$ °C, method 3) and the corresponding XRD pattern are given in Table 2 and Fig. 4(d), respectively. The slight differences observed between the zirconolite XRD patterns for the three methods and for the corresponding lattice parameters could be explained by slight differences in zirconolite crystals composition.

Consequently, the comparison of the three glass-ceramics preparation methods used in this study (glass A) clearly showed that method 3 lead to the highest quantity of zirconolite crystals in the bulk with only a thin titanite + anorthite layer on the surface. Moreover, the small size of the zirconolite crystals obtained following this method is more adapted to minor actinides immobilization because it reduces the risks of fracture of the glass-ceramic

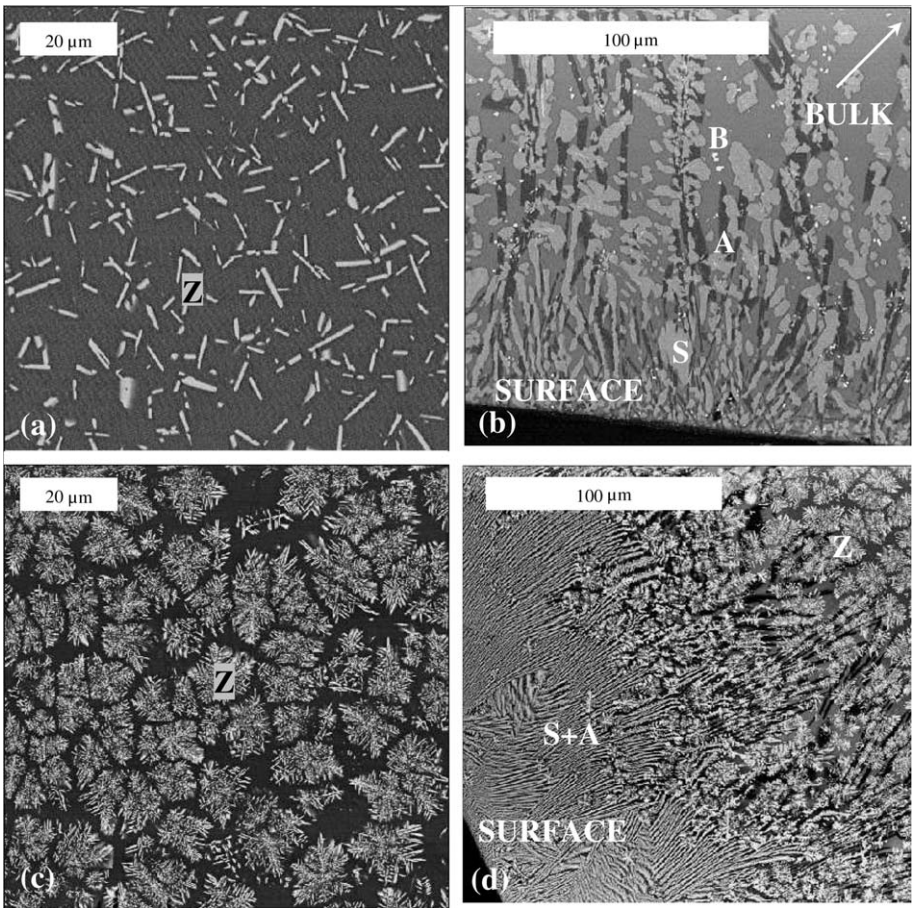

Fig. 6. Back-scattered SEM images of the samples obtained after heat treatment of glass A following method 3 at $T_c = 1200$ °C (bulk (a), near surface (b)) and $T_c = 1050$ °C (bulk (c), near surface (d)). Z, zirconolite; S, titanite; A, anorthite (appearing as the dark phase in (b)); B, badelleyite (appearing as the small size white phase in (b)).

waste forms due to the swelling of the crystals under α-internal irradiation. Nevertheless, method 1 may probably be improved if a zirconolite nucleation stage near 800 °C would be applied to the undercooled melt before the crystal growth thermal treatment at 1050 °C or 1200 °C. Moreover, it must be noticed that small crystals of baddeleyite (ZrO_2) were detected by SEM and EDX in the titanite + anorthite crystallized layer formed at $T_c = 1200$ °C using methods 2 or 3 (Fig. 6(b)). This result is explained in the next paragraph.

3.2. Stability of zirconolite in glass A studied by long thermal treatment

The evolution at high temperature of the nature of the crystalline phases formed in the bulk and near the surface of the glass-ceramics prepared following method 3 are reported in Table 3 for different thermal treatment durations (2–300 h) at $T_c = 1050$ °C and 1200 °C. At 1200 °C, these results clearly

Table 3
Crystalline phases formed in the bulk and near the surface of glass A at $T_c = 1050$ °C and 1200 °C (method 3) for different durations

Crystal growth thermal treatment	Surface	Bulk
2 h 1050 °C	S + A	Z
20 h 1050 °C	S + A + W	Z + A + W + Ap
300 h 1050 °C	S + A + W + C	Z + A + W + S + C + Ap
2 h 1200 °C	S + A + B	Z
20 h 1200 °C	S + A + B	S + A + B + Z[a]

The samples were previously annealed and nucleated at 810 °C for 2 h. (Z, zirconolite; S, titanite; A, anorthite; W, wollastonite; C, cristobalite; B, baddeleyite; Ap, Nd-rich phase probably $Ca_2Nd_8(SiO_4)_6O_2$ apatite).

[a] For this thermal treatment (20 h) the amount of zirconolite in the bulk strongly decreased in comparison with the other treatments presented in the Table.

showed that titanite crystals, occurring initially in a thin crystallized layer near sample surface after 2 h thermal treatment (Fig. 6(b)), have grown towards the bulk at the expense of zirconolite which almost totally disappeared (Fig. 7(a)). This indicated that the zirconolite crystals formed initially in the bulk (Fig. 6(a)) were unstable with respect to titanite and anorthite in the presence of the silica excess of the residual glass at $T_c = 1200$ °C. Thus, at high temperature and for long duration heat treatments, titanite crystals grown from the surface towards the bulk leading to the progressive disappearance of the zirconolite crystals. In this case, the excess of ZrO_2 (which is only partially incorporated in the titanite crystals [23]) precipitated as baddeleyite crystals in the residual undercooled melt (Table 3, Fig. 7(a)). The same phenomena could explain the origin of the baddeleyite crystals observed above in the surface crystallized layer ($T_c = 1200$ °C, Fig. 6(b)). The growth of titanite at the expense of zirconolite could be explained by the existence of a competition between these two phases to incorporate Ti, as it is one of the main elements constituting these two crystalline phases. At 1050 °C, the progress of titanite crystals towards the bulk became very slow in comparison with anorthite (Fig. 7(b)). This can be due to the increase of melt viscosity at 1050 °C, which could slow down the diffusive processes occurring during zirconolite dissolution followed by titanite growth. Even after 300 h at 1050 °C, a high amount of zirconolite remained in the bulk (Table 3, Figs. 8(c) and 7(c)). Moreover, XRD

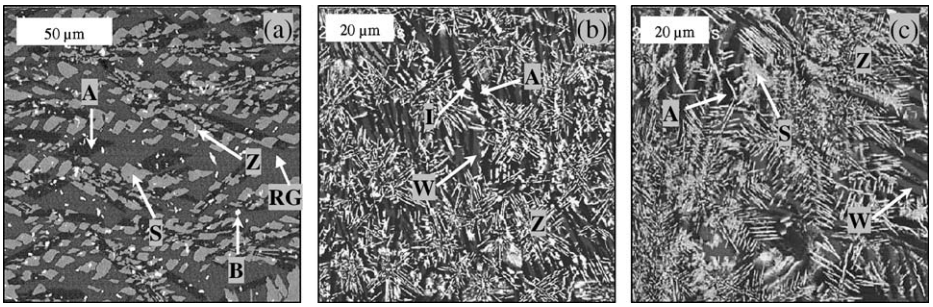

Fig. 7. Back-scattered SEM images of the bulk of the samples obtained after heat treatment of glass A following method 3: (a) $T_c = 1200$ °C 20 h; (b) $T_c = 1050$ °C 20 h; (c) $T_c = 1050$ °C 300 h. Z, zirconolite; S, titanite; A, anorthite (appearing as the dark phase); B, badelleyite (appearing as the small size white phase in (a)); W, wollastonite; I, apatite; RG, residual glass.

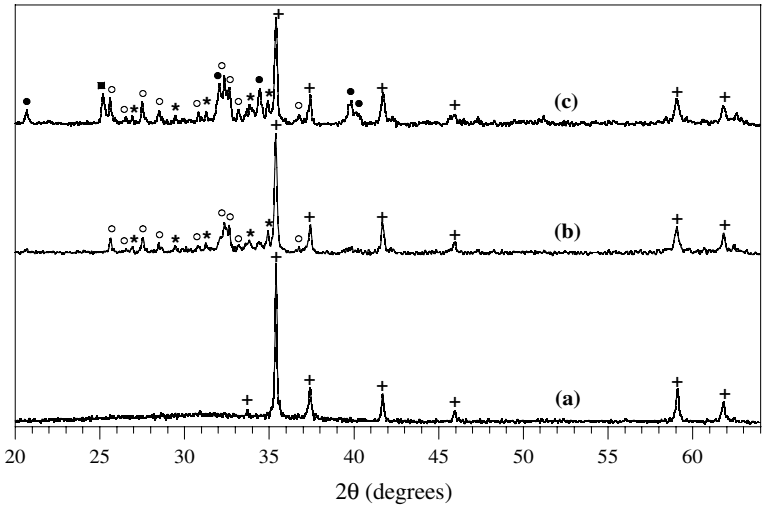

Fig. 8. XRD patterns of the bulk of samples obtained after heat treatments of glass A ($T_c = 1050$ °C) for different durations using method 3: (a) 2 h; (b) 20 h; (c) 300 h. (λCo K_α: 0.178897 nm). +, zirconolite; ○, anorthite; ∗, wollastonite; ●, titanite; ■, cristobalite. The new line occurring after 300 h heating on pattern (c) near $2\theta = 25°$ was attributed to cristobalite because the main line of this phase was known to occur in this angle range.

(Fig. 8(b) and (c)) and EDX indicated the formation of wollastonite crystals (nominally $CaSiO_3$) both in the surface crystallized layer and in the bulk after 20 h or 300 h at $T_c = 1050$ °C (Table 3). The crystallization of this phase was not surprising because of the high amounts of SiO_2 and CaO remaining in the residual glass after titanite, anorthite and zirconolite crystallization. For instance, the amounts (mol.%) of silica and calcium oxide increased from 48.23% (SiO_2) and 25.01% (CaO) in parent glass A to 57.71% (SiO_2) and 25.65% (CaO) in the residual glass in the bulk between zirconolite crystals (method 3, $T_c = 1050$ °C) according to EDX. Wollastonite crystals were probably not stable at 1200 °C in our system which could explain the fact that they were not observed in our samples heat treated at $T_c = 1200$ °C. For the 300 h heat treatment at $T_c = 1050$ °C, the formation of cristobalite was also detected by XRD (Fig. 8(c)) due to the increase of the crystallization of the residual glass for very long durations of heat treatment. Moreover, a very small quantity of a neodymium rich phase was also observed on the SEM images after 20 h and 300 h at $T_c = 1050$ °C (Fig. 7(b), Table 3). Using both EDX and XRD results, it appeared that this phase was probably the $Ca_2Nd_8(SiO_4)_6O_2$ apatite [35].

Thus, the results obtained on glass A for different durations of heat treatment showed that the zirconolite crystals initially formed in the bulk were not stable. Indeed, titanite appeared as the most stable phase incorporating Ti in this case. This phase was also able to incorporate neodymium ions in its structure but less efficiently than zirconolite. Indeed, at $T_c = 1200$ °C (method 3) the composition of the titanite crystals growing from the surface of glass A was determined by EDX: $Ca_{0.89}Nd_{0.11}Ti_{0.69}Zr_{0.22}Al_{0.11}Si_{0.98}O_5$. This formula indicated both that Al^{3+} ions totally compensated the positive charge excess due to the Nd^{3+} ions in the calcium site of titanite (11% of the calcium sites were occupied by neodymium ions) and that a significant amount of Zr^{4+} ions was incorporated in the titanium site. However, for the same sample, the composition of the zirconolite crystals in the bulk (given in Table 1) indicated that Nd^{3+} ions occupied nearly 20% of the calcium sites of the structure. For kinetics reasons due to its relatively high homogeneous nucleation rate $I_Z^{hom}(T)$, zirconolite is the only crystalline phase which nucleated and grown in the bulk. However, studies performed by Vance and Agrawal [36], mixing and firing (at 1280 °C for 2 days) titanite and zirconolite phases (without other silica-rich phase), showed that these two phases were compatible. In our case (glass A), it is probably the occurrence of a silica-rich residual glass coexisting with zirconolite crystals which is at the origin of their instability in comparison with titanite crystals able to incorporate silicon in their structure. In order to reduce the risks of advance of the titanite crystals from the surface of glass A at the expense of the zirconolite crystals formed in the bulk using method 3, T_c must not be too high ($T_c < 1200$ °C) and τ at this temperature must not exceed 20 h. It is very important to underline that if minor actinides ($\leqslant 10$ wt%) were incorporated in such glass-ceramics, the internal temperature of the waste form would never exceed 400 °C during disposal. In this temperature range, zirconolite would thus remain kinetically stable and no long-term evolution of both the structure and microstructure of the glass-ceramics is expected ($T < T_g$).

3.3. Crystallization of apatite from glass B

The optical observation of the sample obtained after controlled cooling of the melt (glass B, method 5) indicated that the amount of crystalline phase (bulk and surface) was very low (i.e., the amount of transparent residual glass remained very high). Moreover, the sample obtained after the nucleation and crystal growth stages from the glassy state (glass B, method 4) was totally opaque. The SEM images and XRD patterns of the samples obtained after thermal treatments of glass B are shown, respectively, in Figs. 9 and 10. It appeared that only one kind of crystalline phase (calcium Nd-silicate apatite) was formed either in the bulk or near the surface of the samples. It is interesting to indicate that recent studies [37,38] concerning the lanthanide oxides (La_2O_3, Gd_2O_3) solubility limit in sodium aluminoborosilicate glass compositions reported the formation of La- and Gd-silicate apatite crystals containing sodium with a composition near $NaGd_9(SiO_4)_6O_2$ for the melt studied in [38]. However, contrary to the composition of glass B, their melts composition did not contain calcium.

The microstructure of the scarce but relatively big crystals formed using method 5 was relatively complex. Fig. 9(a) shows an example of a crystallized region in the bulk of the sample. It looks like a crystals cluster with a nearly hexagonal symmetry whose size reached more than 20 μm but which probably originated from only one nucleating center (nucleus) located initially in the middle of

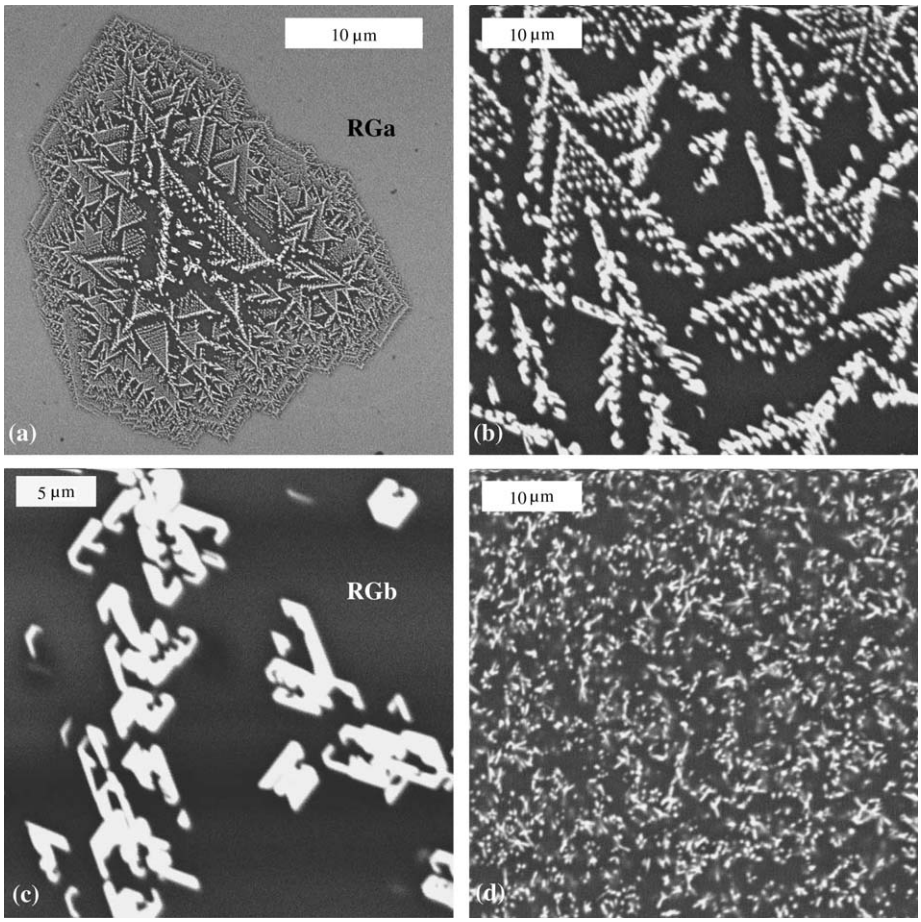

Fig. 9. Back-scattered SEM images of the samples obtained after heat treatment of glass B: (a, b, c) controlled cooling from the melt (6 °C/min) (method 5). Images (a)–(c) correspond to different magnifications of the same crystal of apatite nucleated in the bulk. (d) Nucleation at 640 °C for 2 h and crystal growth at 870 °C for 30 h (method 4). Apatite crystals appear as a white phase (with more or less dendritic shape) on the images because of the heavy element enrichment (Nd) of these crystals in comparison with both residual glass RGb (the phase appearing as a black one near the crystals) and parent glass RGa (which nearly corresponds to the gray phase far from the crystals).

the crystallized region. As the temperature of the melt decreased at a rate of 6 °C/min (method 5), an increase of both its viscosity and of the apatite crystallization driving force occurred during crystal growth because the difference ΔT between the liquidus and the crystal growth temperatures increased. Moreover, during crystal growth, the composition of the undercooled melt changed near the growing interface crystal-melt (the crystallization of apatite was obviously non-congruent in glass B). All these phenomena certainly lead (during crystal growth) to an increase of the diffusion layer thickness near the growing crystal surface that could explain the evolution of the crystals cluster-like microstructure from their center (Fig. 9(c)) to their edge (Fig. 9(b)): evolution from a planar to a dendritic interface [39].

Because of the small amount of crystalline phase, the XRD pattern of the sample obtained following method 5 exhibited low intensity lines (Fig. 10(b)). Comparison of this pattern with the one of $Ca_2Nd_8(SiO_4)_6O_2$ apatite ceramic (Fig. 10(c)) showed that the crystals had an apatite structure. The corresponding lattice parameters are given in Table 4. Only small differences were observed between the parameters of the crystals formed in the glass and the ones of the ceramic. This could be due to slight composition differences. The very small number of crystals observed using method 5 indicated that both surface and bulk nucleation rates of apatite (respectively, $I_{Ap}^{het}(T)$ and $I_{Ap}^{hom}(T)$) were very weak in the temperature range in which apatite crystal growth is high. This showed that apatite crystal growth rate $u_{Ap}(T)$ and nucleation

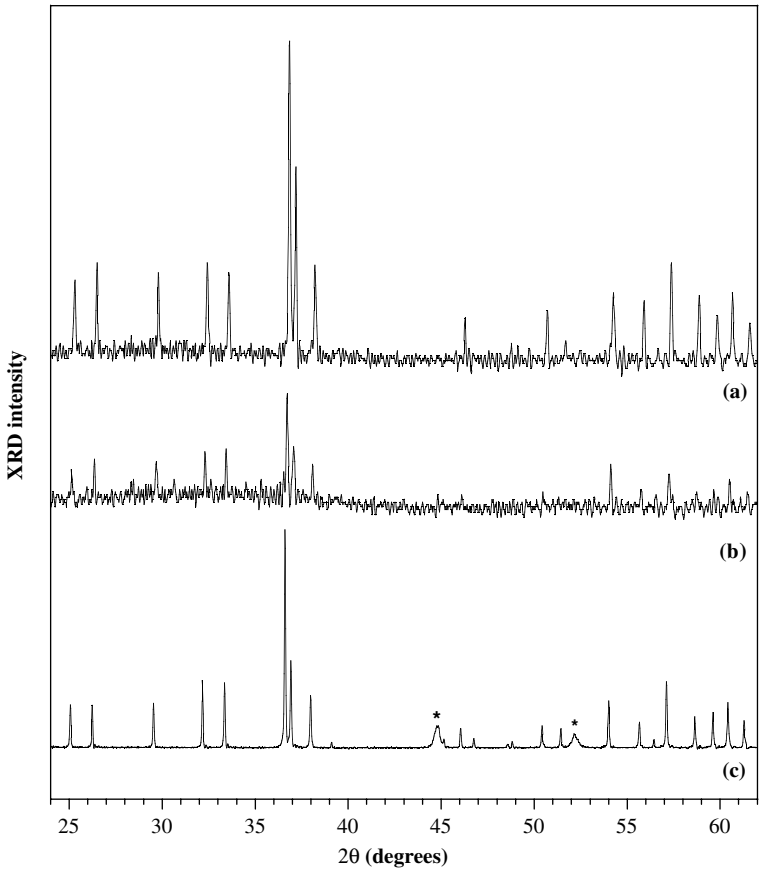

Fig. 10. XRD patterns of the samples obtained after heat treatments of glass B: (a) nucleation at 640 °C for 2 h and crystal growth at 870 °C for 30 h (method 4); (b) controlled cooling from the melt (6 °C/min) (method 5). For comparison the XRD pattern of the $Ca_2Nd_8(SiO_4)_6O_2$ apatite ceramic is shown (c) with the following lattice parameters ($P63/m$ space group): $a = 0.95225(5)$ nm and $c = 0.70200(4)$ nm (numbers in parentheses are standard deviations and applied to the last quoted place). The method used to prepare the ceramic sample is given in the legend of Table 4 ∗: lines due to the aluminum support. Patterns (a) and (b) can be indexed in the $P63/m$ hexagonal system and are very similar to the pattern of the ceramic (c). (λCo K_α: 0.178897 nm).

Table 4
Unit cell parameters ($a = b$, c, and volume cell V) of the apatite crystals formed in glass B using methods 4 and 5

	$a = b$ (nm)	c (nm)	V (nm^3)
Apatite (method 4)	0.9519(1)	0.7010(1)	0.5502(2)
Apatite (method 5)	0.9527(2)	0.7007(2)	0.5508(4)
Apatite (glass C)	0.95212(5)	0.70096(6)	0.5503(1)
Apatite (ceramic)	0.9522(5)	0.70200(4)	0.5513(1)

These parameters were deduced from the indexation of the XRD patterns (Fig. 10) in the $P63/m$ space group. For comparison the cell parameters of the $Ca_2Nd_8Si_4O_{26}$ ceramic and of the apatite crystals formed in glass C using method 4 are also given. This ceramic was prepared by solid state reaction from oxides and carbonates at 900 °C for 24 h (first sintering) and then at 1300 and 1400 °C for 24 h (second and third sinterings) followed by a final heat treatment at 1500 °C for 100 h (fourth sintering) in order to obtain single phase apatite ceramic. Grinding and peletizing were performed between the different sintering stages. Numbers in parentheses are standard deviations and applied to the last quoted place.

rates $I_{Ap}^{het}(T)$ and $I_{Ap}^{hom}(T)$ occurred in different temperature ranges (i.e., $(I_{Ap}^{het}(T), I_{Ap}^{hom}(T))$ and $u_{Ap}(T)$ curves did not significantly overlap). Because of the small size of the apatite crystals it was not possible to determine precisely their composition by EDX or EPMA. However, the EDX spectrum

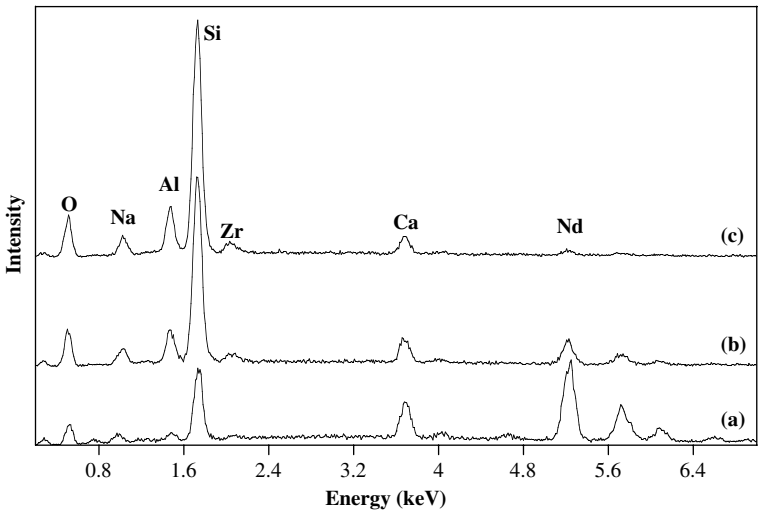

Fig. 11. EDX spectra of the sample obtained after heat treatment (controlled cooling from the melt (6 °C/min)) of glass B: (a) apatite phase (appearing as the white phase in Fig. 9(c)), (b) residual glass RGa far from the crystals (it nearly corresponds to parent glass, Fig. 9(a)), (c) residual glass RGb near the crystals (Fig. 9(c)). The three spectra were recorded using the same conditions (accelerating voltage: 15 kV, acquisition time: 100 s, spot analysis). The position of the stronger line of the different elements is indicated in the figure. The detection of low intensity signals near 1.0 keV (Na region), 1.5 keV (Al region) and 2.0 keV (Zr region) for the apatite crystal (Fig. 11(a)) are probably due to the contribution of a small amount of residual glass RGb during analysis because of the small size of the crystals (Fig. 9(c)).

(Fig. 11(a)) of the center of the crystals (Fig. 9(c)) confirmed that they are mainly constituted of Nd_2O_3, SiO_2 and CaO. The detection of low intensity EDX signals that could be attributed to Na, Al and Zr in Fig. 11(a) are probably due to the contribution of a small amount of residual glass RGb around the crystals (Fig. 9(c)). Nevertheless, EPMA was performed on the apatite crystals formed in another glass (glass C) containing both more Na_2O and CaO and less Al_2O_3 contents than glass B. Glass C lead to large apatite crystals after slow cooling of the melt (1 °C/min) and exhibited an XRD pattern very similar to the one of the crystals formed in glass B after cooling at 6 °C/min (Fig. 10(b)). EPMA showed that their composition was approximately $Ca_{2.48}Nd_{7.68}Si_{6.00}O_{26}$ [26]. This suggests that the composition of the apatite crystals formed in glass B is probably not very different to the composition of this calcium apatite. It can be underlined that, in spite of the relatively high Na_2O concentration in glasses B and C in comparison with CaO concentration (for example in glass B the amounts (mol.%) of Na_2O and CaO were, respectively, 12.40 and 5.44), sodium does not significantly enter into the apatite crystals. This could be surprising because a sodium apatite phase $NaNd_9Si_6O_{26}$ was described in literature [40] and the corresponding ceramic can be prepared easily by solid state reaction. Several propositions can be given to explain the fact that Na^+ ions did not enter significantly into the apatite crystals formed during cooling of the melt (glasses B and C):

– In a recent study performed on two glass compositions (glasses D and E) not very different to the one of glass B, we showed that the total substitution of CaO by Na_2O (glass E did not contain CaO) lead to the crystallization of $NaNd_9Si_6O_{26}$ in glass E [41]. However, the sodium apatite nucleation rate in glass E was considerably lower than the one of $Ca_2Nd_8Si_6O_{26}$ crystals in glass D containing both CaO and Na_2O. The lowest tendency of sodium apatite to crystallize during melt cooling in comparison with calcium apatite could be due to lowest tendency of Na^+ ions to separate from the silicate melt and to associate with Nd^{3+} ions to lead to apatite crystallization. Indeed, it is known that the tendency of modifier cations (Na^+, Ca^{2+}, Nd^{3+} ions in the present work) to separate from glasses or from melts increases with their field strength F [42]. F can be defined as $F = Z/d^2$ where Z is the cation charge and d is mean distance cation–oxygen of the first coordination shell. In our case we evaluated: $F_{Nd} = 4.8 \times 10^{-3}$ nm^{-2} from our previous EXAFS results on glass B [43] and $F_{Ca} = 3.6 \times 10^{-3}$ nm^{-2} and $F_{Na} = 1.8 \times 10^{-3}$ nm^{-2} from [44]. This could

explain the highest nucleation rate of Ca-apatite in comparison with Na-apatite. Another possibility is that the Gibbs free energy ΔG_f of formation of the Ca-apatite is lower than the one of the Na-apatite (i.e., the Ca-apatite is thermodynamically more stable than the Na-apatite). Then, the crystallization driving force and the nucleation rate of the Ca-apatite would probably be higher for this phase. In order to test this hypothesis it would be necessary to perform thermodynamic measurements for these two apatite phases prepared for instance as single-phase ceramics.

– The different structural role of Na^+ and Ca^{2+} cations in the glass (as modifiers near non-bridging oxygen atoms or as charge compensator near AlO_4^- or BO_4^- units) and thus their different locations in glass structure, could be also at the origin of the preferential crystallization of Ca-apatite in glass B. Indeed, recent NMR (Nuclear Magnetic Resonance) results indicated that Na^+ ions would compete favorably with Ca^{2+} ions for aluminum and boron tetrahedra charge compensation [45,46]. Moreover, in [43,26] we showed that neodymium cations were mainly located in the depolymerized regions of the glass B network i.e., in regions containing high concentrations of non-bridging oxygens. Consequently, the amount of sodium cations available to associate with neodymium cations in the depolymerized regions and to lead to the nucleation of sodium-apatite crystals, is lower than the total amount of sodium ions in the composition. This non-equivalent repartition of Na^+ and Ca^{2+} cations in glass structure (and probably also in the melt during controlled cooling) would favor the simultaneous occurrence of calcium and neodymium ions in the same regions of the glassy network and thus would tend to facilitate calcium apatite crystallization.

The EDX pattern (Fig. 11(c)) of the residual glass in the center of the apatite microstructure (appearing as the dark phase called RGb in Fig. 9(c)) clearly showed a strong neodymium depletion in comparison with residual glass (RGa in Fig. 9(a)) far from the crystals (Fig. 11(b)). Residual glass RGa had a composition almost similar to the one of parent glass B. This result is in agreement with the contrast differences observed on the back-scattered electron images (Fig. 9(a) and (c)).

Fig. 9(d) shows the SEM image of the sample obtained after nucleation + crystal growth of glass B (method 4). A very high number of small and thin crystals (size < 5 μm) was observed, which demonstrated that the nucleation stage at $T_n = 640$ °C was very efficient. In this case, the microstructure of the sample was very similar to the one of classical glass-ceramics that contained a very high density of small crystals dispersed homogeneously in the bulk. Contrary to glass A (method 3) which lead to the nucleation and growth of different phases in the bulk (zirconolite) and near the surface (titanite + anorthite), XRD showed that only one kind of crystals (apatite) formed in glass B even after 30 h thermal treatment at $T_c = 870$ °C. T_c was chosen in agreement with the DTA curve of glass B (Fig. 2) which showed that the exothermic peak B1 associated with apatite crystallization occurred near 880 °C. Due to their too small size, it was not possible to perform EDX analysis on apatite crystals. However, the XRD pattern of the sample obtained using method 4 (Fig. 10(a)) was very similar to the one of the crystals formed during controlled cooling (method 5, Fig. 10(b)). The lattice parameters of the apatite phase formed in the sample obtained following method 4 are given in Table 4. It appears that these parameters are very similar to the one of the apatite crystals formed in glass C after controlled cooling. The slight deviations observed between the parameters $a = b$ of the apatite crystals formed in glass B using methods 4 and 5 are probably due to small differences of crystals composition.

In comparison with the results obtained for glass A (20–300 h thermal treatment at T_c) – which showed that zirconolite was less stable at high temperature (T_c) than the titanite phase growing from the surface and thus lead to its progressive disappearance – the results obtained for glass B showed that in the undercooled melt (when its viscosity was low enough to enable crystal growth) apatite was a stable phase. Indeed, the crystallization of another phase (for instance from sample surface) that would then lead to the disappearance of apatite was not observed for glass B.

3.4. Partitioning of Nd between crystals and residual glass

It is interesting to compare the composition of the residual glass for the samples containing apatite or zirconolite crystals. For glass A, after the nucleation (T_n) + crystal growth (T_c) heat treatment, the composition of the residual glass between zirconolite crystals (Fig. 6(a) and (c)) was

determined by EDX [35]. It appeared that Nd_2O_3 concentration (mol.%) decreased only from 1.27 to 1.20 and from 1.27 to 0.98 for $T_c = 1200$ °C and 1050 °C, respectively. This small decrease of Nd_2O_3 concentration in residual glass was in accordance with the results concerning glass A presented in another paper [32]: using EPR (electron paramagnetic resonance) we showed that only 24% and 36% of all the neodymium of glass A was incorporated in the zirconolite phase for $T_c = 1200$ °C and 1050 °C, respectively. However, increasing TiO_2 and ZrO_2 concentrations in glass A composition, we showed it was possible to incorporate nearly 43% of all neodymium in the zirconolite phase (57% of all Nd_2O_3 still remaining in the residual glass of glass-ceramics). Concerning glass B, Fig. 11 shows that near the apatite crystals the residual glass was strongly neodymium depleted (compare spectra (b) and (c)). This suggested that the amount of Nd_2O_3 remaining in the residual glass near zirconolite crystals (glass A) was probably higher than in the residual glass near apatite crystals formed in glass B. The apatite-based glass-ceramics are thus more efficient to concentrate lanthanides in the crystalline phase. This will be also the case for trivalent minor actinides (Am^{3+}, Cm^{3+}) if we admit that neodymium is a good surrogate as stated in the Introduction. The highest efficiency to segregate Nd in glass-ceramics prepared from glass B is not really surprising because neodymium ions occupied only a small fraction of the cation sites in zirconolite structure (Nd^{3+} occupied only 20% of the Ca^{2+} sites for the crystals formed in glass A) whereas Nd^{3+} ions occupied 80% of the cation sites available in the apatite crystals formed in glass B. Using the cell volume V and the composition of the zirconolite and apatite ceramics prepared in this work (respectively, $Ca_{0.8}Nd_{0.2}ZrTi_{1.8}Al_{0.2}O_7$ ($V = 1.0119\ nm^3$) and $Ca_2Nd_8Si_4O_{26}$ ($V = 0.5513\ nm^3$)) that are very similar to the ones of the crystals formed in glasses A and B, respectively, (Tables 2 and 4), we can calculate the concentration of Nd^{3+} ions in the apatite and zirconolite crystals: 1.87 Nd^{3+} ions/nm^{-3} (zirconolite) and 14.5 Nd^{3+} ions/nm^{-3} (apatite). In the glass-ceramics studied in this work, apatite is thus able to concentrate eight times more Nd^{3+} ions than zirconolite.

The best partitioning ratio of Nd^{3+} ions between the residual glass and the crystals in the apatite-based glass-ceramics must be tempered by the fact that previous works [27] indicated that the chemical durability of $Ca_2Nd_8Si_4O_{26}$ was lower than the one of zirconolite. This result can be explained by the fact that SiO_2 is more soluble in water than both TiO_2 and ZrO_2. The high lixiviation resistance of zirconolite was conserved even after amorphization of its structure under α self-irradiation. Indeed, after about 3×10^{25} α-decays/m^3, dissolution tests performed in water at 90 °C showed that amorphized ^{244}Cm doped $CaZrTi_2O_7$ ceramic exhibited two orders of magnitude better retention of curium than amorphized ^{244}Cm doped $Ca_2Nd_8Si_4O_{26}$ ceramic [27]. Moreover, the saturation macroscopic swelling under α self-irradiation was shown to be higher for apatite (9.4 vol.%) than for zirconolite (7.1 vol.%) [47]. However, recent studies using heavy ions irradiation showed that phospho-silicated fluoroapatite $Ca_{10-x}Nd_x(SiO_4)_x(PO_4)_{6-x}F_2$ ceramics exhibited increasing resistance to amorphization when x decreased (i.e., when the amount of PO_4 groups in the apatite structure increased) [48]. It was also demonstrated that the phosphofluoroapatite $Ca_{10}(PO_4)_6F_2$ was more resistant to external irradiations than the lanthanum silicate apatite $Ca_2La_8Si_4O_{26}$ [47]. It could be thus interesting to try to prepare glass-ceramics containing $Ca_{10-x}Nd_x(SiO_4)_x(PO_4)_{6-x}F_2$ ($x > 0$) crystals introducing both phosphorus and fluorine in the parent glass composition.

4. Conclusions

The crystallization of two silicate glass compositions (A and B) either during heat treatment of the glass or slow cooling of the melt was studied. It appeared that the combination of a nucleation stage near T_g with a crystal growth stage lead to the efficient crystallization in the bulk of zirconolite ($Ca_{0.8}Nd_{0.2}ZrTi_{1.8}Al_{0.2}O_7$) and apatite ($Ca_2Nd_8Si_6O_{26}$), respectively, for A and B glasses. Independently on the method used to induce crystallization, apatite was the only phase nucleating in glass B. In glass A, zirconolite was the only phase nucleating in the bulk after 2–4 h but other phases (titanite $CaTiSiO_5$, anorthite $CaAl_2Si_2O_8$) can nucleate heterogeneously on glass surface.

For glass A and for relatively short crystal growth thermal treatments ($\tau = 2$ h), conclusions concerning the relative values of the homogeneous (bulk) and heterogeneous (surface) nucleation rates of the different crystalline phases (zirconolite, titanite and anorthite) were drawn. For longer duration ($\tau = 20$–300 h) of crystal growth thermal treatments at high temperature (1200 °C), the zirconolite crystals initially formed in the bulk disappeared at the

expense of the titanite crystals nucleated on glass A surface. Consequently, in the system studied in this work, zirconolite was not thermodynamically stable in comparison with titanite. However, for kinetics reasons due to its relatively high homogeneous nucleation rate, zirconolite was the only crystalline phase that nucleated and grew in the bulk. It is important to underline that during disposal, the temperature in the bulk of such waste form would never exceed 400 °C even with 10 wt% MA (Cm isotopes – that would be mainly responsible for the heating – represent less than 10 wt% of all MA). In this temperature range ($T < 400$ °C), zirconolite would remain kinetically stable and no long-term evolution of both the structure and microstructure of the glass-ceramics are expected ($T < T_g$). However, the main problem of the zirconolite-based glass-ceramics studied in this work was that a great part of Nd remained in the residual glass: more than 50% of Nd was not incorporated in zirconolite crystals even if TiO_2 and ZrO_2 contents were increased in parent glass.

For glass B, although $[Na_2O] > [CaO]$, sodium did not significantly enter into the apatite structure. Considerations concerning both the modifier cations field strength and the non-equivalent repartition of Na^+ and Ca^{2+} cations in glass structure were proposed to explain the preferential crystallization of Ca-apatite. The apatite-based glass-ceramics obtained were more efficient to concentrate lanthanides in the crystalline phase than the zirconolite crystals in glass A. The partitioning ratio of Nd between apatite and residual glassy phases was not determined, but EDX analysis showed that it was higher than for the zirconolite-based glass-ceramics. Nevertheless, according to literature, the apatite crystals formed in glass B did not exhibit as good long-term behavior as zirconolite.

Acknowledgements

The financial support by the CEA, by the COGEMA and by the GDR Nomade for this work is gratefully acknowledged. The authors are thankful to Dr L. Robbiola (ENSCP, France) for his help during SEM and EDX measurements.

References

[1] B. Boullis, Retraitement et séparation des radionucléides à vie longue, in: R. Turlay (Ed.), Les déchets nucléaires, Les Editions de Physique, France, 1997, p. 69.
[2] R. Guillaumont, C. R. Chim. 7 (2004) 1129.
[3] C. Lopez, PhD Thesis, Université Paris XI (France), 2002.
[4] C. Madic, M. Lecomte, P. Baron, B. Boullis, C. R. Phys. 3 (2002) 797.
[5] C. Guy, F. Audubert, J.-E. Lartigue, C. Latrille, T. Advocat, C. Fillet, C. R. Phys. 3 (2002) 827.
[6] C. Fillet, T. Advocat, F. Bart, G. Leturcq, H. Rabiller, C. R. Chim. 7 (2004) 1165.
[7] I.W. Donald, B.L. Metcalfe, R.N.J. Taylor, J. Mater. Sci. 32 (1997) 5851.
[8] N. Dacheux, N. Clavier, A.-C. Robisson, O. Terra, F. Audubert, J.-E. Lartigue, C. Guy, C. R. Chim. 7 (2004) 1141.
[9] I. Muller, W.J. Weber, Mater. Res. Soc. Bull. (September) (2001) 698.
[10] P. Loiseau, D. Caurant, N. Baffier, C. Fillet, Mater. Res. Soc. Symp. Proc. 757 (2003) 243.
[11] E.R. Vance, A. Jostsons, R.A. Day, C.J. Ball, B.D. Begg, P.J. Angel, Mat. Res. Soc. Symp. Proc. 412 (1996) 41.
[12] W.J. Weber, Radiat. Eff. 77 (1983) 295.
[13] E.R. Vance, C.J. Ball, B.D. Begg, M.L. Carter, R.A. Day, G.J. Thorogood, J. Am. Ceram. Soc. 86 (2003) 1223.
[14] R.G. Haire, N.A. Stump, Mat. Res. Soc. Symp. 465 (1997) 39.
[15] G.K. Liu, V.V. Zhorin, M.R. Antonio, S.T. Li, C.W. Williams, L. Soderholm, J. Chem. Phys. 112 (2000) 1489.
[16] R.D. Shannon, Acta Crystallogr. A32 (1976) 751.
[17] C. Lopez, X. Deschanels, C. Den Auwer, J.-N. Cachia, S. Peuget, J.-M. Bart, Phys. Scr. T115 (2005) 342.
[18] J.-N. Cachia, PhD Thesis, Université Montpellier II (France), 2005.
[19] P. Loiseau, D. Caurant, N. Baffier, L. Mazerolles, C. Fillet, Mater. Res. Soc. Symp. Proc. 663 (2001) 179.
[20] P. Loiseau, D. Caurant, N. Baffier, C. Fillet, Mater. Res. Soc. Symp. Proc. 663 (2001) 169.
[21] P. Loiseau, D. Caurant, I. Bardez, O. Majerus, N. Baffier, C. Fillet, Mater. Res. Soc. Symp. Proc. 757 (2003) 281.
[22] P. Loiseau, D. Caurant, O. Majerus, N. Baffier, L. Mazerolles, C. Fillet, Phys. Chem. Glasses 43C (2002) 195.
[23] P. Loiseau, D. Caurant, O. Majerus, N. Baffier, C. Fillet, J. Mater. Sci. 38 (2003) 843.
[24] P. Loiseau, D. Caurant, N. Baffier, L. Mazerolles, C. Fillet, J. Nucl. Mater. 335 (2004) 14.
[25] I. Bardez, D. Caurant, J.L. Dussossoy, P. Loiseau, C. Gervais, F. Ribot, D.R. Neuville, N. Baffier, C. Fillet, Nucl. Sci. Eng. 153 (2006) 1.
[26] I. Bardez, PhD Thesis, Université ParisVI (France), 2004.
[27] J.W. Wald, W.J. Weber, in: G. Wicks, W.A. Ross (Eds.), Advances in Ceramics Nuclear Waste Management, vol. 8, The Am. Ceram. Soc, Columbus, OH, 1984, p. 71.
[28] C. Fillet, J. Marillet, J.L. Dussossoy, F. Pacaud, N. Jacquet-Francillon, J. Phalippou, Ceram. Trans. 87 (1997) 531.
[29] P.F. James, Nucleation in glass-forming systems a review, in: J.H. Simmons, D.R. Uhlmann, G.H. Beall (Eds.), Nucleation and Crystallization in Glasses, Advances in Ceramics, vol. 4, The Am. Ceram. Soc., Columbus, OH, 1982, p. 1.
[30] N.H. Ray, J. Non-Cryst. Solids 15 (1974) 423.
[31] P.J Hayward, Glass-ceramics, in: W. Lutze, R.C. Ewing (Eds.), Radioactive Waste Forms for the Future, Elsevier, 1988, p. 427.
[32] P. Loiseau, D. Caurant, O. Majerus, N. Baffier, C. Fillet, J. Mater. Sci. 38 (2003) 853.
[33] Z. Strnad, Glass-Ceramic Materials, Elsevier, 1986, p. 9.

[34] P.C. Kong, G.A. Reimann, J. Environ. Sci. Health A32 (1997) 1207.
[35] P. Loiseau, PhD Thesis, Université ParisVI (France), 2001.
[36] E.R. Vance, D.K. Agrawal, Nucl. Chem. Waste Manage. 3 (1982) 229.
[37] L. Li, D.M. Strachan, H. Li, L.L. Davis, M. Qian, J. Non-Cryst. Solids 272 (2000) 46.
[38] D. Zhao, L. Li, L.L. Davis, W.J. Weber, R.C. Ewing, Mater. Res. Soc. Symp. Proc. 663 (2001) 199.
[39] G.W. Scherer, Glass formation and relaxation, in: R.W. Cahn, P. Haasen, E.J. Kramer (Eds.), Materials Science and Technology: A Comprehensive Treatment, Glasses and Amorphous Materials, vol. 9, VCH, 1991, p. 119.
[40] J. Felsche, J. Solid State Chem. 5 (1972) 266.
[41] D. de Ligny, D. Caurant, I. Bardez, J.L. Dussossoy, P. Loiseau, D.R. Neuville, Atalante 2004: advances for future nuclear fuel cycles. (Nîmes, 2004 France), in: Proceedings of the Congress (CD-ROM), 2004.
[42] O.V. Mazurin, G.P. Roskava, E.E. Porai-Koshits, Phase Separation in Glass, Elsevier Science Publishers, 1984, p. 108.
[43] I. Bardez, D. Caurant, P. Loiseau, J.L. Dussossoy, C. Gervais, F. Ribot, D.R. Neuville, N. Baffier, Phys. Chem. Glasses 46 (2005) 320.
[44] G.E. Brown, F. Farges, G. Calas, Rev. Miner. 32 (1995) 317.
[45] H. Yamashita, K. Inoue, T. Nakajin, H. Inoue, T. Maekawa, J. Non-Cryst. Solids 331 (2003) 128.
[46] F. Angeli, PhD Thesis, Université Paris VII (France), 2000.
[47] W.J. Weber, R.C. Ewing, C.R. Catlow, T. Diaz de la Rubia, L.W. Hobbs, C. Kinoshita, Hj. Matze, A.T. Motta, N. Nastasi, E.KH. Salje, E.R. Vance, S.J. Zinkle, J. Mater. Res. 13 (1998) 1434.
[48] S. Soulet, J. Carpena, J. Chaumont, O. Kaitasov, M.-O. Ruault, J.-C. Krupa, Nucl. Intrum. and Meth. B 184 (2001) 383.